NATIONAL ADVISORY COMMITTEE FOR AERONAUTICS

TECHNICAL NOTE 3535

FLIGHT INVESTIGATION OF THE SURFACE-PRESSURE DISTRIBUTION AND THE FLOW FIELD AROUND A CONICAL AND TWO SPHERICAL NONROTATING FULL-SCALE PROPELLER SPINNERS

By Jerome B. Hammack, Milton L. Windler,
and Elwood F. Scheithauer

Langley Aeronautical Laboratory
Langley Field, Va.

Washington
September 1955

NATIONAL ADVISORY COMMITTEE FOR AERONAUTICS

TECHNICAL NOTE 3535

FLIGHT INVESTIGATION OF THE SURFACE-PRESSURE DISTRIBUTION AND THE FLOW FIELD AROUND A CONICAL AND TWO SPHERICAL NONROTATING FULL-SCALE PROPELLER SPINNERS

By Jerome B. Hammack, Milton L. Windler, and Elwood F. Scheithauer

SUMMARY

A flight investigation has been made on three nonrotating full-scale propeller spinners at free-stream Mach numbers of 0.70 to 0.96 to determine the surface-pressure distribution and the magnitude and radial extent of the influence of each spinner on the local flow field. One spinner was a conventional conical spinner. The other two spinners had conical forebodies and spherical midsections that provided a mechanically simple means of affording an aerodynamically clean blade seal.

The departure from stream conditions in the propeller plane of the conical spinner and the 60° spherical spinner extended beyond the 1.3-spinner-radius station; whereas, with the 45° spherical spinner, stream conditions were reached at the 1.3-spinner-radius station. High peak negative pressure coefficients occurred over the spherical section of both spherical spinners between the cone-sphere juncture and the blade center line. The local surface Mach numbers in this region are approximately 0.4 higher than that at free-stream Mach number of 0.95. The effect of yaw on both the surface-pressure distribution and the local flow field was investigated over the top and bottom surfaces of the 45° spherical spinner and was found to be small for the test conditions.

Unfavorable flow separation occurred over the rear portion of the spherical spinners. This flow separation caused mild buffeting of the airplane above a free-stream Mach number of 0.72 with the 60° spherical spinner and above 0.83 with the 45° spherical spinner.

INTRODUCTION

The present trend in propeller design is toward wide blades of high solidity, and analytical studies and wind-tunnel tests indicate that such propellers maintain good efficiency at transonic and supersonic speeds. In these studies and tests, however, the blades are faired into the spinners to form smooth junctures with no provision for pitch change. In actual flight where pitch changes are necessary, the wide blades of transonic and supersonic propellers create a complex problem of effecting a good spinner juncture. A common approach to the solution of this problem is to fair the blade rapidly to a round section before entering the spinner. Investigations (refs. 1 and 2) have shown that the transition for the free blade to round sections at the blade shank causes an appreciable loss in propeller efficiency. The ideal aerodynamic approach is to continue the efficient blade sections to the spinner surface. The mechanical problems associated with propeller-blade sealing, however, are much more difficult when this approach is used.

A mechanically simple means by which a smooth juncture is obtained has been studied by the National Advisory Committee for Aeronautics; a mock-up of a spherical spinner-blade combination which illustrates the principle involved is shown in figure 1. The blade is mounted on a sphere which has had the front portion cut off and replaced by a cone and has had the rear section removed for fit with the fuselage. The blade is fitted to a seal that is clamped to and rotates with the blade so that at all blade angles the spherical surface is maintained.

A flight research program to investigate propeller blades using spinners that incorporate spherical sections so that there will be no aerodynamic penalties arising from changes in juncture geometry has been undertaken. Three nonrotating spinner configurations were fabricated and investigations of the air flows over these spinners were made. These three spinners were a conventional conical design, a spinner with a 17.5-inch-radius spherical center section and a 60° conical section, and a spinner with a 15.2-inch-radius spherical center section and a 45° conical section. The purpose of this paper is to present the results of flight investigations of the surface-pressure distribution and flow field around the three nonrotating full-scale spinner configurations.

Calculations of the values of local Mach number are based on the assumptions of no shock formation off the spinner and constant values of total pressure. These assumptions are considered to be valid for values of first-order magnitude.

SYMBOLS

H	total pressure, lb/sq ft
p	static pressure, lb/sq ft
q_c	free-stream impact pressure, $H_o - p_o$, lb/sq ft
$\frac{\Delta p}{q_c}$	static-pressure coefficient, $\frac{p_l - p_o}{q_c}$
M	Mach number
ψ	angle of yaw, deg
l	maximum spinner length, in.
r	radius from spinner center line, in.
r_b	spinner radius at blade center line, in.
x	distance along spinner center line, in.
y	distance from spinner surface, in.

$z = r_b + y$, in.

Subscripts:

o	free stream
l	local

SPINNER CONFIGURATIONS

Three nonrotating full-scale dummy propeller spinners were constructed and tested in flight on a propeller research airplane. The details of the conventional conical propeller spinner are shown in figure 2. The other two spinners had spherical midsections and were very similar except that one had a cone angle of 60° (see fig. 3) and the other had a cone angle of 45° (see fig. 4). These spinners are designated the 60° spherical spinner and the 45° spherical spinner, respectively. Photographs of the three spinners installed on the test airplane are presented as figures 5 to 7.

INSTRUMENTATION

Surface-pressure measurements.- The static-pressure distributions over the upper and lower surfaces of each spinner were obtained by measuring the difference in static pressure between each spinner orifice and a reference static pressure obtained from a 1-chord-length wing-tip airspeed installation using standard NACA pressure recorders. The position error of the reference static-pressure system was found to be negligible over the Mach number range by previous tests on the airplane. Pressure-lag errors in the static-pressure lines resulting from rapid changes in altitude were avoided by conducting the tests at relatively constant altitude.

Measurement of the local static-pressure field.- The local static-pressure field around each spinner was measured at the blade center-line station (figs. 2 to 4) with static-pressure survey rakes installed on the 10° and 190° meridians of the conical spinner, the 356° and 176° meridians of the 60° spherical spinner, and the 350° and 170° meridians of the 45° spherical spinner. (The 0° meridian is on the upper surface and the angles are measured clockwise as seen from the front of the airplane.) These rakes were offset from the vertical plane to avoid interference with the surface-pressure measurements. The probes on each rake were located the following distances from the spinner surface: 0.5, 1.0, 1.5, 2.5, 3.5, and 5.5 inches (fig. 5). Each probe was referenced to the static-pressure source that was used for the surface-pressure measurements.

The survey-rake installation on the spinners was made with the static-pressure probes alined with the local surface. The possibility of rake misalinement with the local flow was investigated on the 60° spherical spinner at free-stream Mach numbers of 0.40 and 0.58 by bending the third and fifth probe on each rake inward 10° toward the spinner surface. Although this bending moved the probes into a more negative static-pressure field, the increase in negative pressure measured was greater than that which should result from a change in probe distance from the spinner surface alone; thus, bending the probes introduced a position error into the measured static pressure. The original installation with the probes parallel to the local surface (fig. 6) was used during the tests since the rakes were more nearly alined with the flow. The flow-misalinement error of this installation is probably within 5° and the resulting error in pressure coefficient is of the order of 1 percent.

Measurement of angles of attack and yaw.- The conical forebodies of the spinners were utilized to measure the angle of attack α by use of

the following relationship:

$$\alpha = \frac{1}{k} \frac{\Delta p'}{q_c}$$

where $\Delta p'$ is the pressure differential between orifices on the upper and lower surfaces at the same value of x/l and k is an experimental constant based on reference 3 and unpublished wind-tunnel data. A constant of 0.0360 was used for the conical spinner, 0.0450 for the 60° spherical spinner, and 0.0386 for the 45° spherical spinner. For angles of yaw, the same values of k were used but the pressure differential was taken between the 90° and 270° meridians. The errors in the angles of attack and yaw were estimated to be within ±0.5°.

TESTS

The local static-pressure field over the spinners was investigated at Mach numbers of 0.70 to 0.96 and altitudes between 20,000 and 33,000 feet by measuring the surface-pressure distribution and the local static-pressure field around the spinner.

The effect of yaw on the flow field around the 45° spherical spinner was investigated at M_o of 0.65 by sideslipping the airplane to obtain yaw variations of approximately ±5°.

RESULTS

Surface Static-Pressure Distributions

Conical spinner.- The static-pressure distribution over the surface of the conical spinner is presented in figure 8 as the variation of static-pressure coefficient $\Delta p/q_c$ with orifice station x/l for flight Mach numbers from 0.70 to 0.96. Each curve was obtained by averaging the static pressures measured along the 0° and 180° meridians in order to compensate for the effect of angle of attack which varied from about 0.5° to 1.6° throughout the tests. Angles of yaw during the tests did not exceed ±0.7° and were considered to have no appreciable effect on the measurements.

45° spherical spinner.- The variation of static-pressure coefficient $\Delta p/q_c$ with orifice location x/l for flight Mach numbers from 0.75 to 0.96 are shown in figure 9 for the 45° spherical spinner. Where

it was possible to obtain values of the 0°- and 180°-meridian orifices the data were averaged; some points, however, represent the pressures obtained at only one orifice. (The points at which there is only one orifice are shown in fig. 4.) The differences due to the angle-of-attack variations experienced in the tests were found to be small. The effect of yaw up to ±5° on the measured static pressures at a Mach number of 0.65 is shown in figure 10. At the higher test Mach numbers, the amount of yaw experienced in the tests was of the order of 1° and was neglected.

60° spherical spinner.- The static-pressure variations over the surface of the 60° spherical spinner for flight Mach numbers from 0.70 to 0.95 are presented in figure 11. Because this spinner had the largest cone angle of the three spinners tested, the differences in pressures measured along the 0° and 180° meridians were relatively large, and both sets of measurements are presented.

Radial Variation of Local Mach Number

Along Blade Center Line

Conical spinner.- The influence of the conical spinner on the local Mach number at the blade center line is presented in figure 12 as the variation of the ratio of local Mach number to flight Mach number M_l/M_o with radial position z/r_b for flight Mach numbers of 0.70 to 0.96. The values presented are the average between the rakes on the 10° and 190° meridians in order to compensate for the effect of angle of attack. The angle-of-yaw variation was small and its effect was negligible.

45° spherical spinner.- The local Mach number variation M_l/M_o with radial position z/r_b along the blade center line is presented in figure 13 for flight Mach numbers from 0.75 to 0.96. The curves are averages for the 350° and 170° meridians and the effect of angle of attack is small. The effect of yaw on the local Mach number distribution is presented in figure 14 for angles of yaw of about 5°. At the higher Mach numbers presented in figure 13, the angle of yaw was about 1°.

60° spherical spinner.- The local Mach number variation M_l/M_o with radial position z/r_b along the blade center line is presented for flight Mach numbers of 0.70 to 0.95 in figure 15. The curves presented are for the 356° and 176° meridians since there is a relatively large difference between the upper and lower rakes.

DISCUSSION

Surface-Static-Pressure Distribution

Some features of the static-pressure distributions over the three spinners could be anticipated from theory and wind-tunnel tests. For example, the conical spinner has peak positive pressure coefficients at the nose which decrease as the flow accelerates over the spinner (fig. 8). This is also true for the conical forebodies of the two spherical spinners. The increases in cone angle result in more positive pressure coefficients. The spherical center sections of these spinners cause high peak negative pressures between the cone-sphere juncture and the blade center line (figs. 9 to 11). The magnitude of these peak pressure coefficients is approximately the same for both the 45° and 60° spherical spinners at corresponding Mach numbers. Blockage of the lower spinner surface by the air inlet and the oil cooler duct and a small angle-of-attack effect have a larger influence on the 60° spherical spinner than on the other two spinners; this influence is reflected in the variation between the 0°- and 180°-meridian pressure coefficients. The effect of yaw was found to be small on the 45° spherical spinner.

The flow is supersonic in the peak-negative-pressure region above $M_0 = 0.75$ on both spherical spinners. The flow is decelerating rapidly over the rear portion of the spherical spinners and eventually becomes subsonic again. In this rear region, the 45° spherical spinner has pressure coefficients which are more positive by about 0.1 at all forward-flight Mach numbers than those on the 60° spherical spinner.

Separation occurs over the discontinuities at the rear of the spherical spinners and causes very mild buffeting at the higher flight Mach numbers. Buffeting occurred at M_0 above 0.72 with the 60° spherical spinner and above 0.83 with the 45° spherical spinner. A trend common to all three spinners over the region forward of the blade center line is the tendency toward more positive pressure coefficients with increases in flight Mach number. A comparison of the maximum local Mach numbers at $M_0 = 0.95$ shows that the spherical spinners have about a M_l of 1.35 and the conical spinner has a M_l of 0.84 (at the blade center line).

Radial Variation of Local Mach Number

Along Blade Center Line

The 45° spherical spinner produces a local Mach number increase at the 1.03-spinner-radius station of less than 5 percent of that of the free stream at the higher test Mach numbers and reaches free-stream velocity at

about the 1.3-spinner-radius station. The departure from free-stream conditions of both the conical spinner and the 60° spherical spinner still exists at the 1.3-spinner-radius station. However, the local Mach number variation for the conical spinner is still relatively small, being of the order of 10 to 15 percent lower than that of the free-stream Mach number. The 60° spherical spinner has local Mach numbers higher than the free-stream Mach numbers by 15 to 35 percent; this condition would alter the thrust distribution of the propeller blade if it were not accounted for.

Another point to be noted in local Mach number variation of the 60° spherical spinner is the large difference between the 356°- and the 176°-meridian rakes. This difference is believed to be due to the fact that the flow below the spinner where the air and oil cooler inlets have a greater effect is different from that on the other two spinners.

Yaw has a large effect on the rakes on the 45° spherical spinner but, at the small yaw angles experienced during the tests (except for those specifically designed to investigate yaw), yaw effects are assumed to be negligible. This assumption applies to the conical and 60° spherical spinners also.

CONCLUDING REMARKS

The surface-static-pressure distribution and the magnitude and radial extent of the influence of each spinner on the local flow field around a full-scale nonrotating conical spinner, a 45° spherical spinner, and a 60° spherical spinner were determined in flight at Mach numbers from 0.70 to 0.96.

The data presented herein are especially useful in determining inboard pitch distributions of blades to be operated with spinners of similar shape. In some cases, the alteration of local flow may be of sufficient magnitude to cause negative section angles of attack if its effect is not accounted for.

The departure from free-stream conditions of the conical and 60° spherical spinners in the propeller plane extended beyond the 1.3-spinner-radius station whereas, with the 45° spherical spinner, stream conditions were reached at the 1.3-spinner-radius station.

Langley Aeronautical Laboratory,
National Advisory Committee for Aeronautics,
Langley Field, Va., July 5, 1955.

REFERENCES

1. Hammack, Jerome B.: Investigation of Thrust Losses Due to Shanks of a Flared-Shank Two-Blade Propeller on a Slender-Nose Airplane. NACA TN 1414, 1947.

2. Delano, James B., and Carmel, Melvin M.: Effect of Shank Design on Propeller Performance at High Speeds. NACA ARR L6D23, 1946.

3. McClanahan, Herbert C., Jr.: Wing-Flow Investigation of a 45° Cone as an Angle-of-Attack Measuring Device at Transonic Speeds. NACA RM L51E16, 1951.

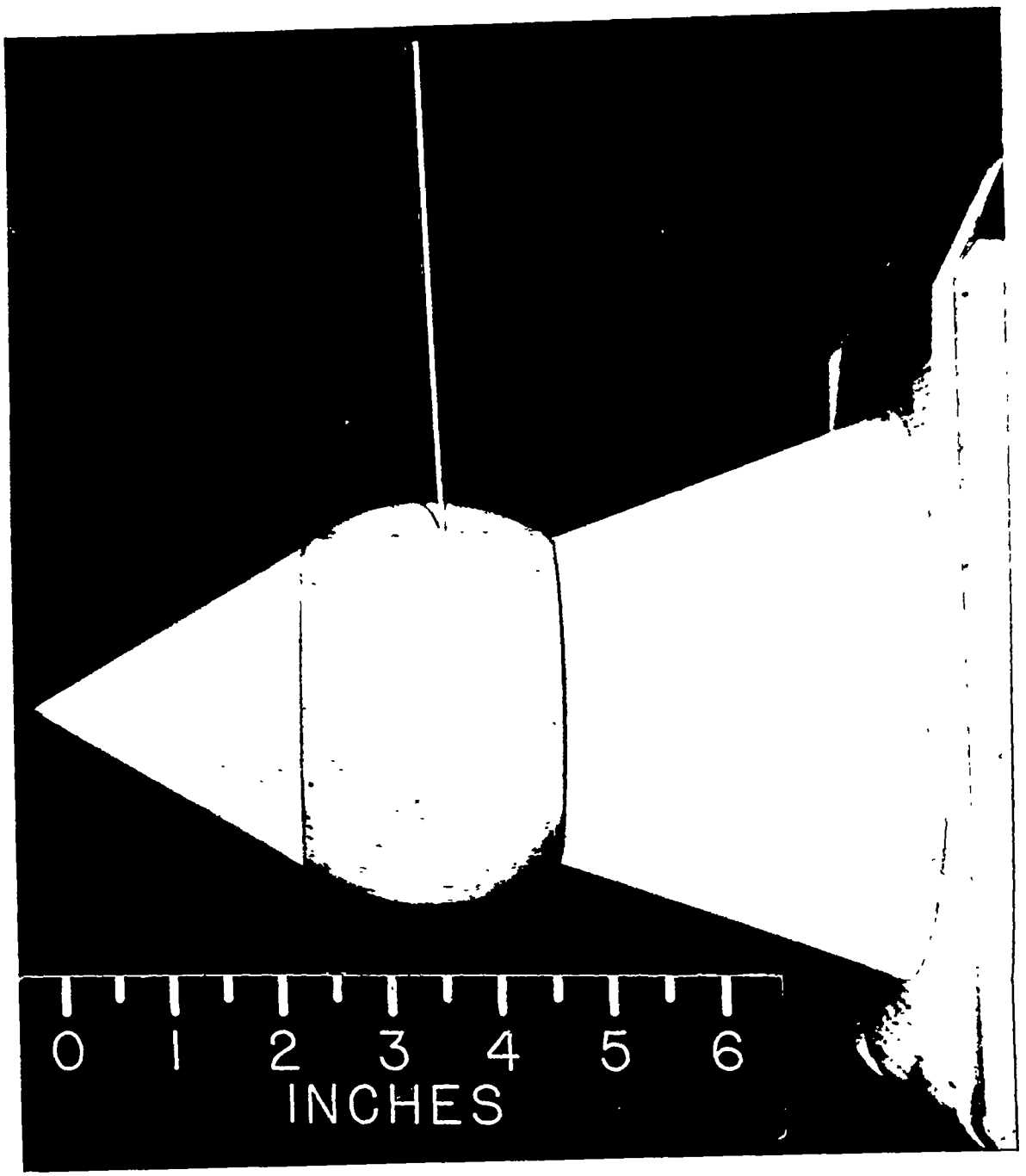

L-70883

Figure 1.- Mock-up of a spherical spinner-blade combination.

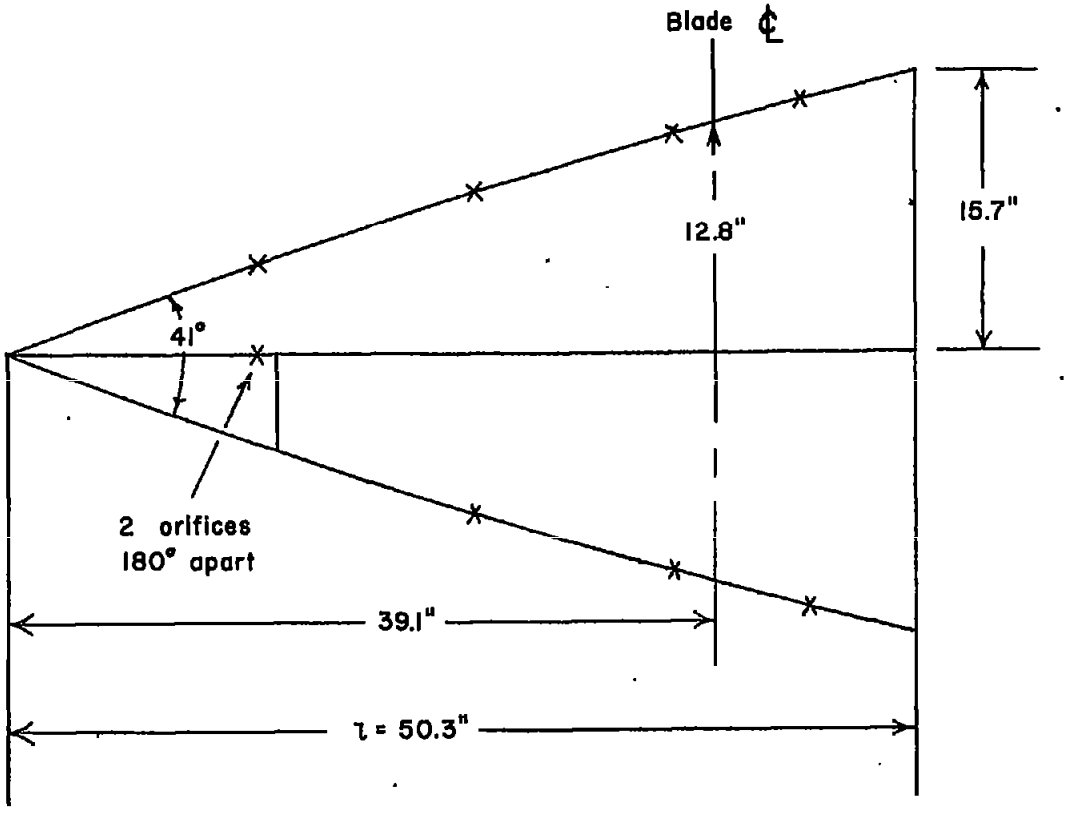

Orifice locations (marked x)						
x, in.	r, in.	x/l	Meridian lines			
			0°	90°	180°	270°
14.0	5.1	0.278	x	x		x
26.0	9.1	.517	x		x	
37.0	12.3	.737	x		x	
44.0	14.0	.875	x		x	

Figure 2.- Dimensions and orifice locations of the conical propeller spinner.

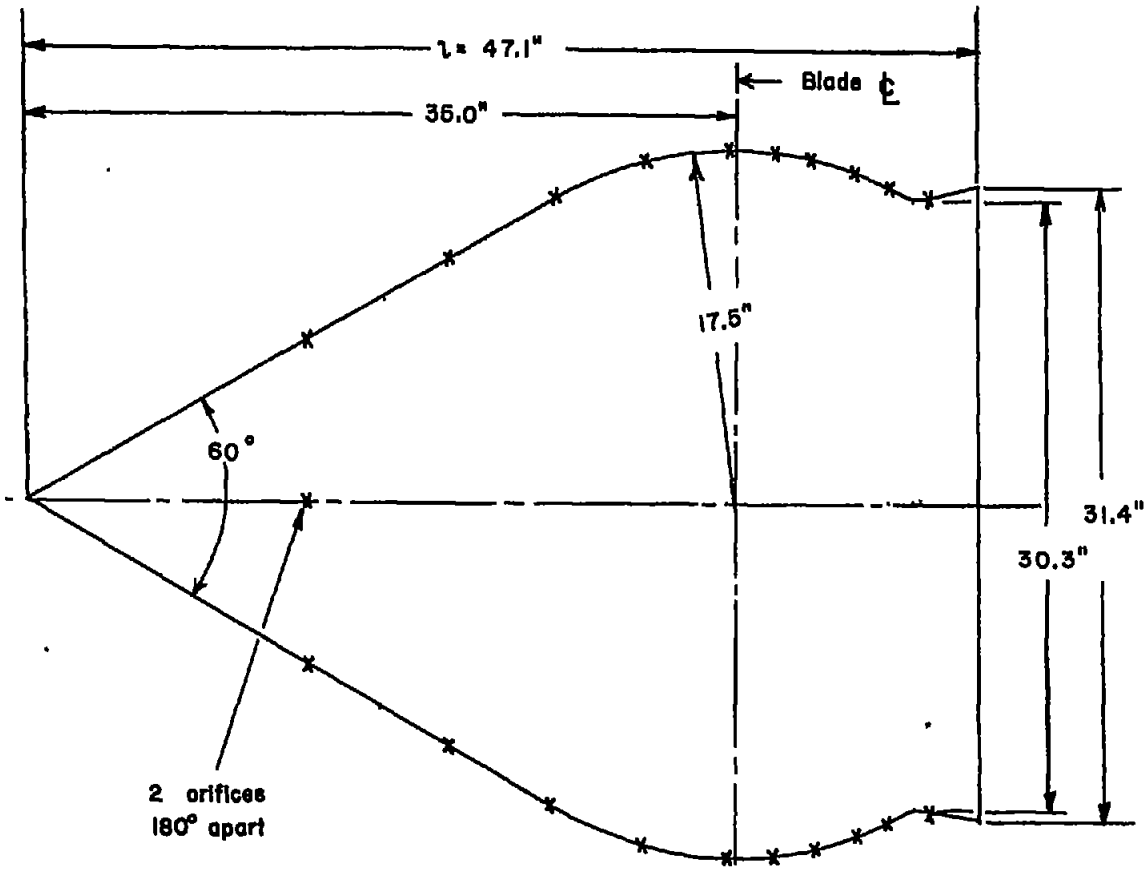

Orifice locations (marked x) for 0° and 180° meridians

x, in.	r, in.	x/l
13.9	8.0	0.295
20.8	12.0	.442
26.0	15.0	.552
30.5	16.9	.648
34.6	17.4	.736
37.0	17.5	.785
39.0	17.1	.829
41.1	16.4	.873
42.9	15.7	.910
44.3	15.3	.940

Figure 3.- Diagram of the 60° spherical spinner showing the orifice locations and the spinner dimensions.

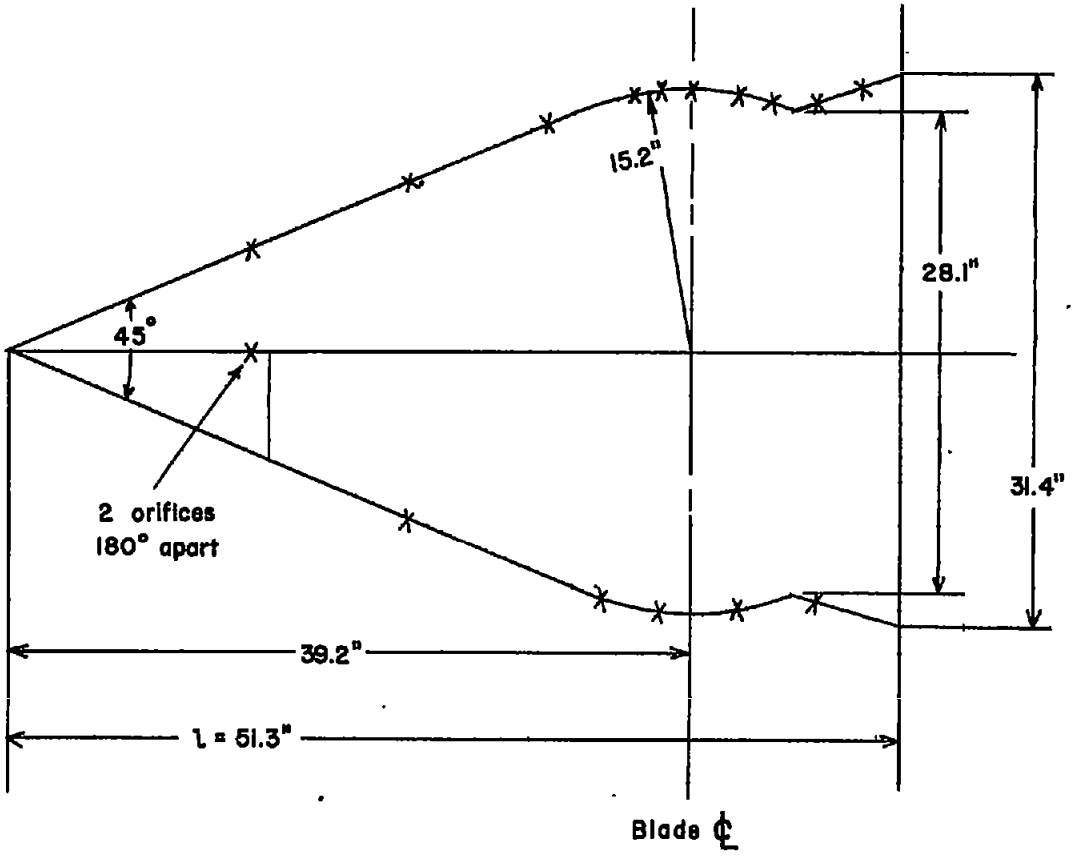

Orifice locations (marked x)						
x, in.	r, in.	x/l	Meridian lines			
			0°	90°	180°	270°
14.0	6.0	0.273	x	x		x
23.0	9.8	.448	x		x	
31.0	13.3	.605	x			
34.2	14.4	.661			x	
36.0	14.9	.702	x			
37.5	15.1	.732	x		x	
39.2	15.2	.765	x			
42.0	14.9	.819	x		x	
44.0	14.5	.858	x			
46.5	14.5	.907	x		x	
49.0	15.4	.955	x			

Figure 4.- Diagram of the 45° spherical spinner showing the orifice locations and the spinner dimensions.

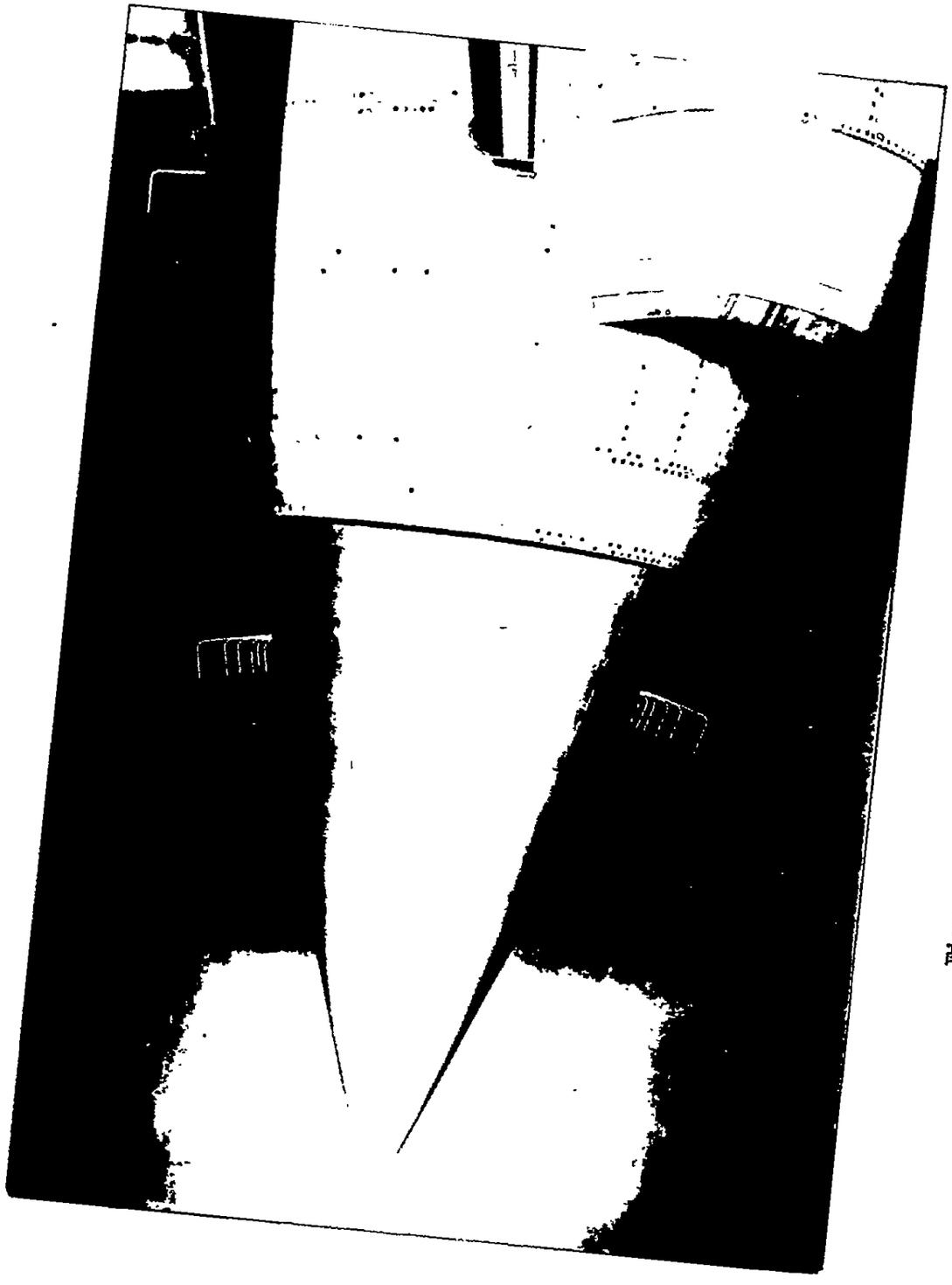

L-85870.1

Figure 5.- Nonrotating conical spinner.

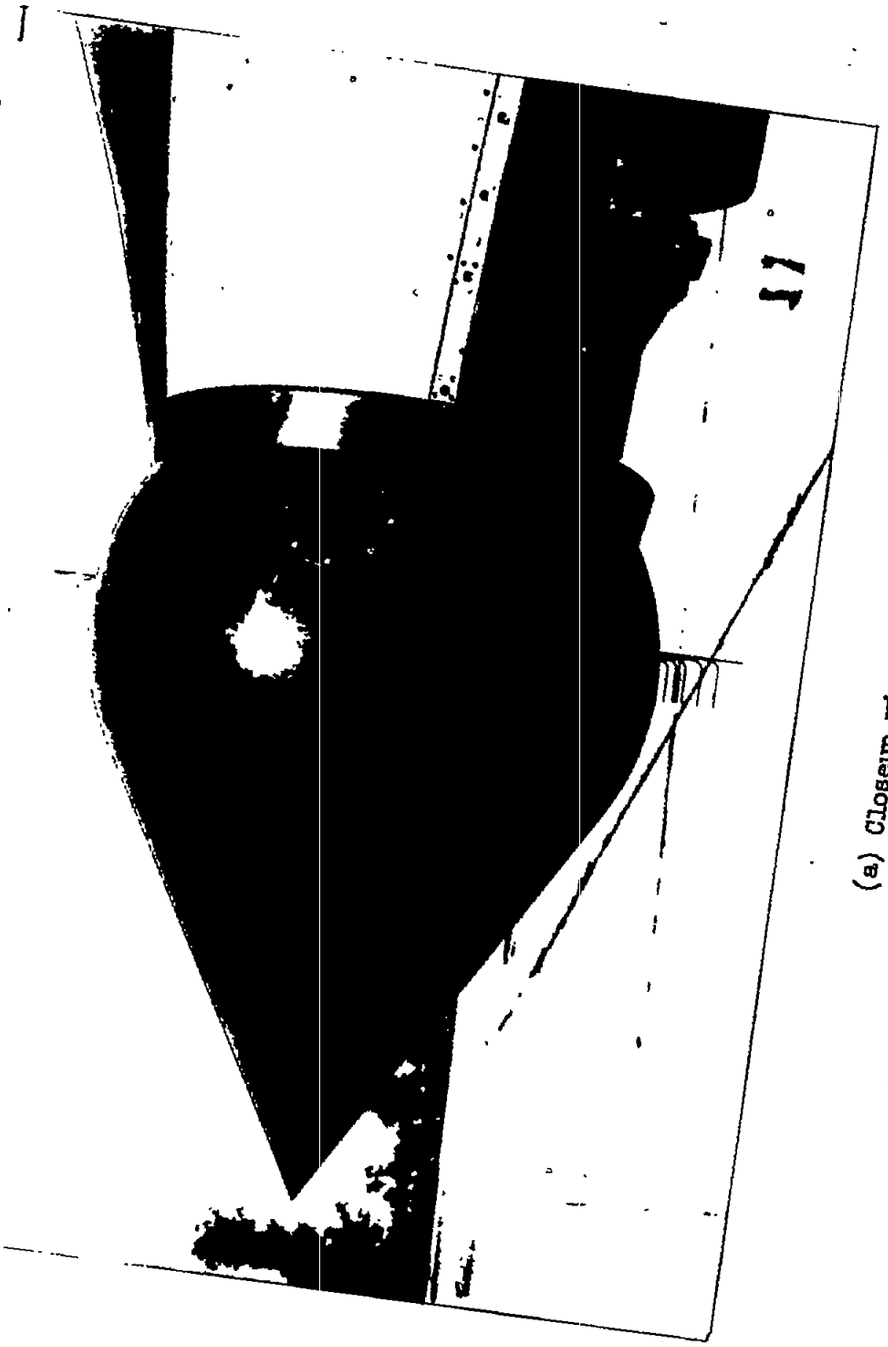

(a) Closeup view. L-84587

Figure 6.- Nonrotating 60° spherical spinner.

L-83952

(b) Spinner installed on propeller research vehicle.

Figure 6.- Concluded.

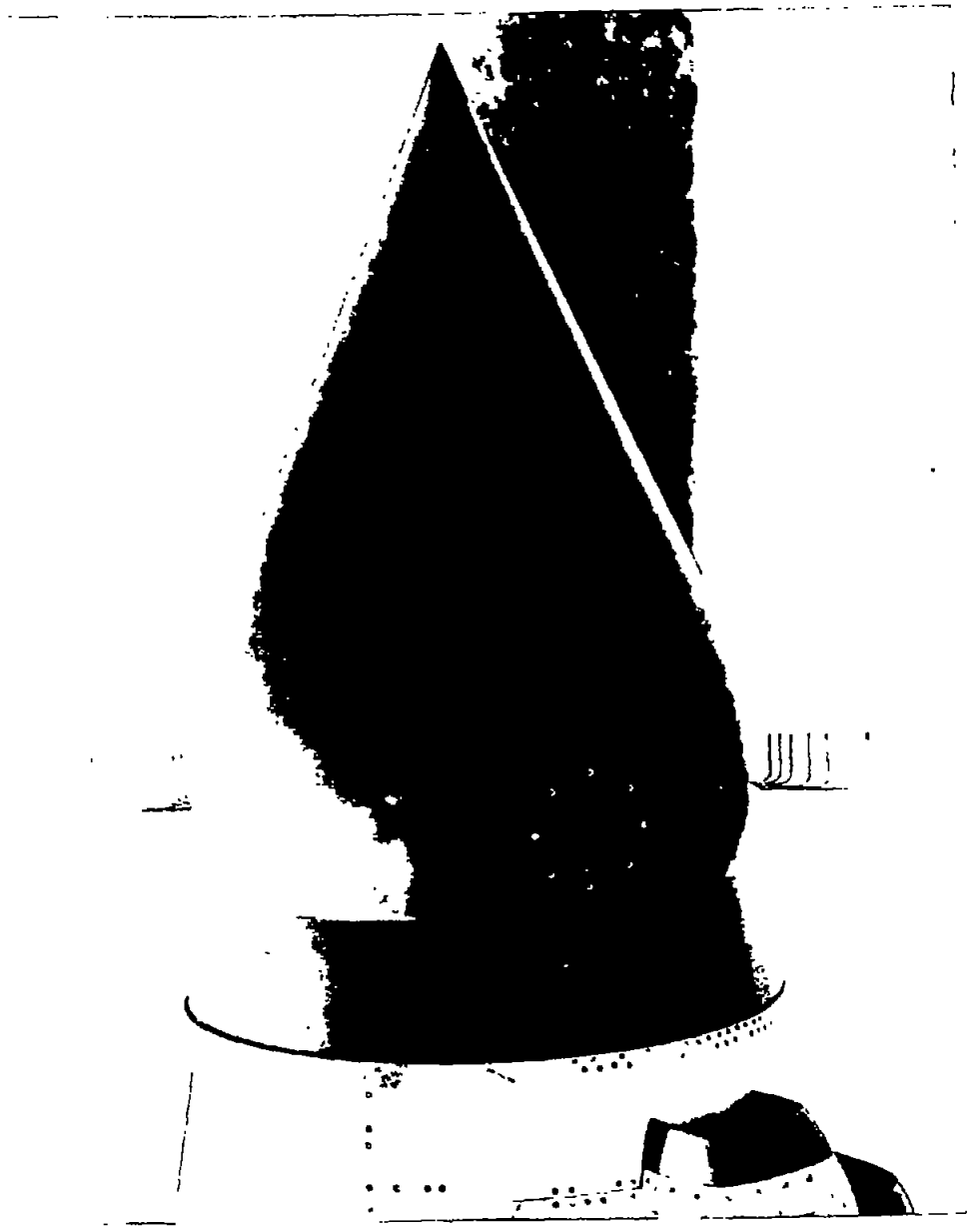

L-85523

(a) Closeup view.

Figure 7.- Nonrotating 45° spherical spinner.

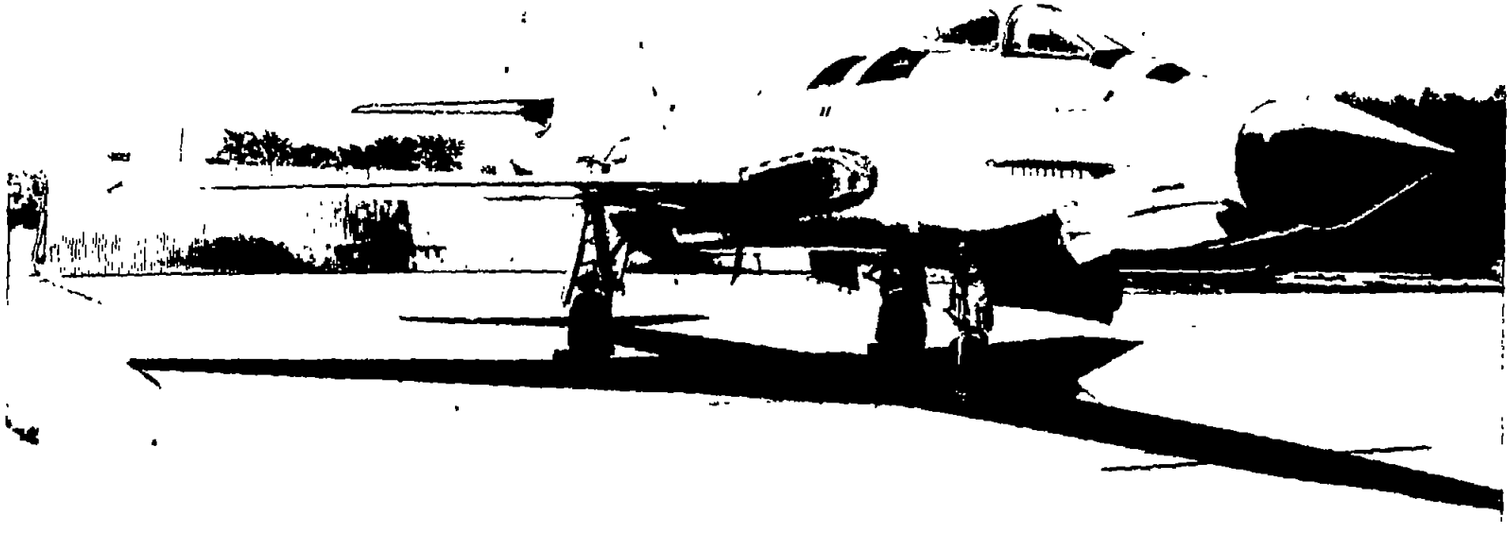

L-85525

(b) Spinner installed on propeller research vehicle.

Figure 7.- Concluded.

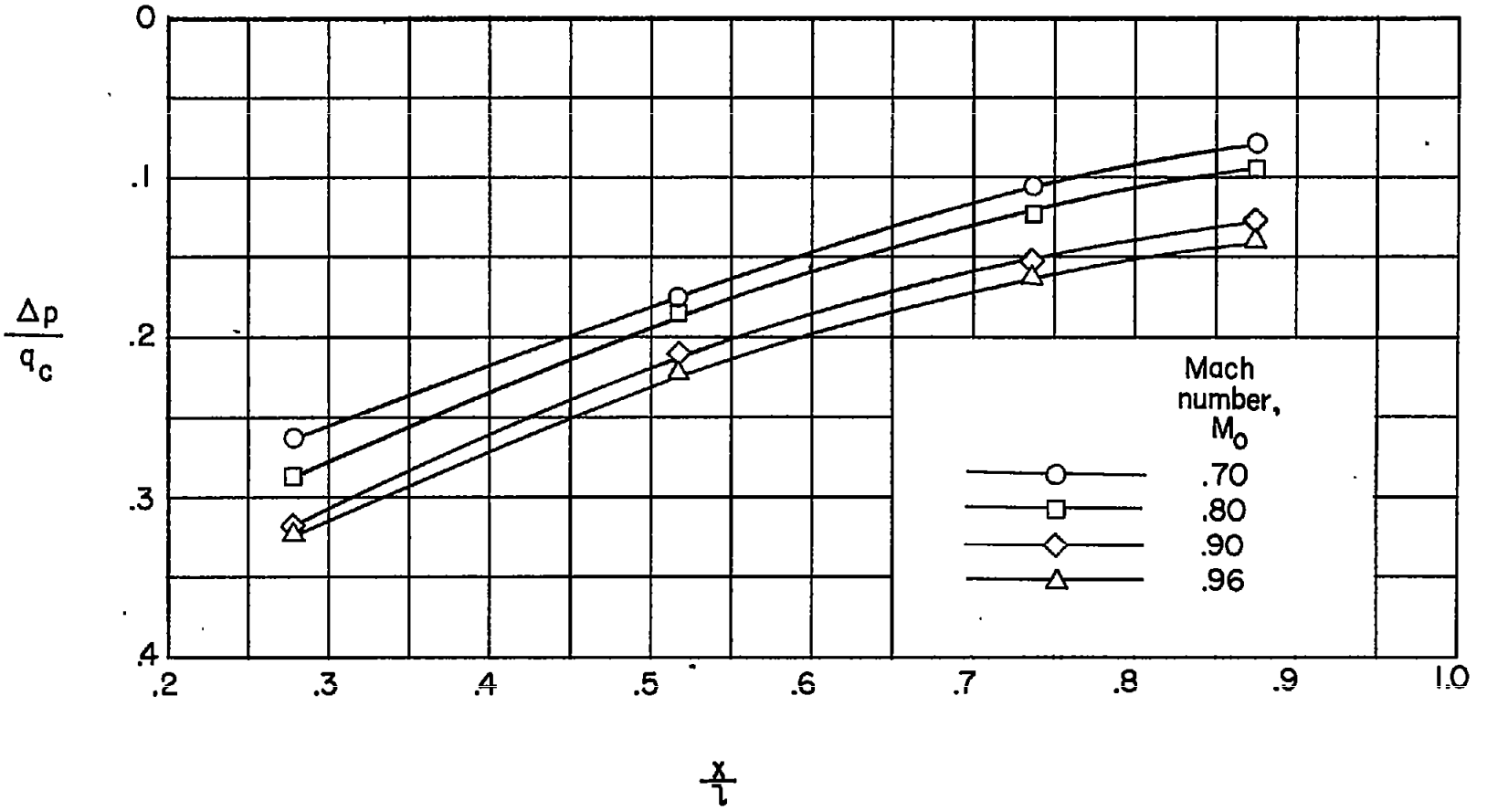

Figure 8.- Effect of Mach number on the pressure distribution over the surface of the conical spinner.

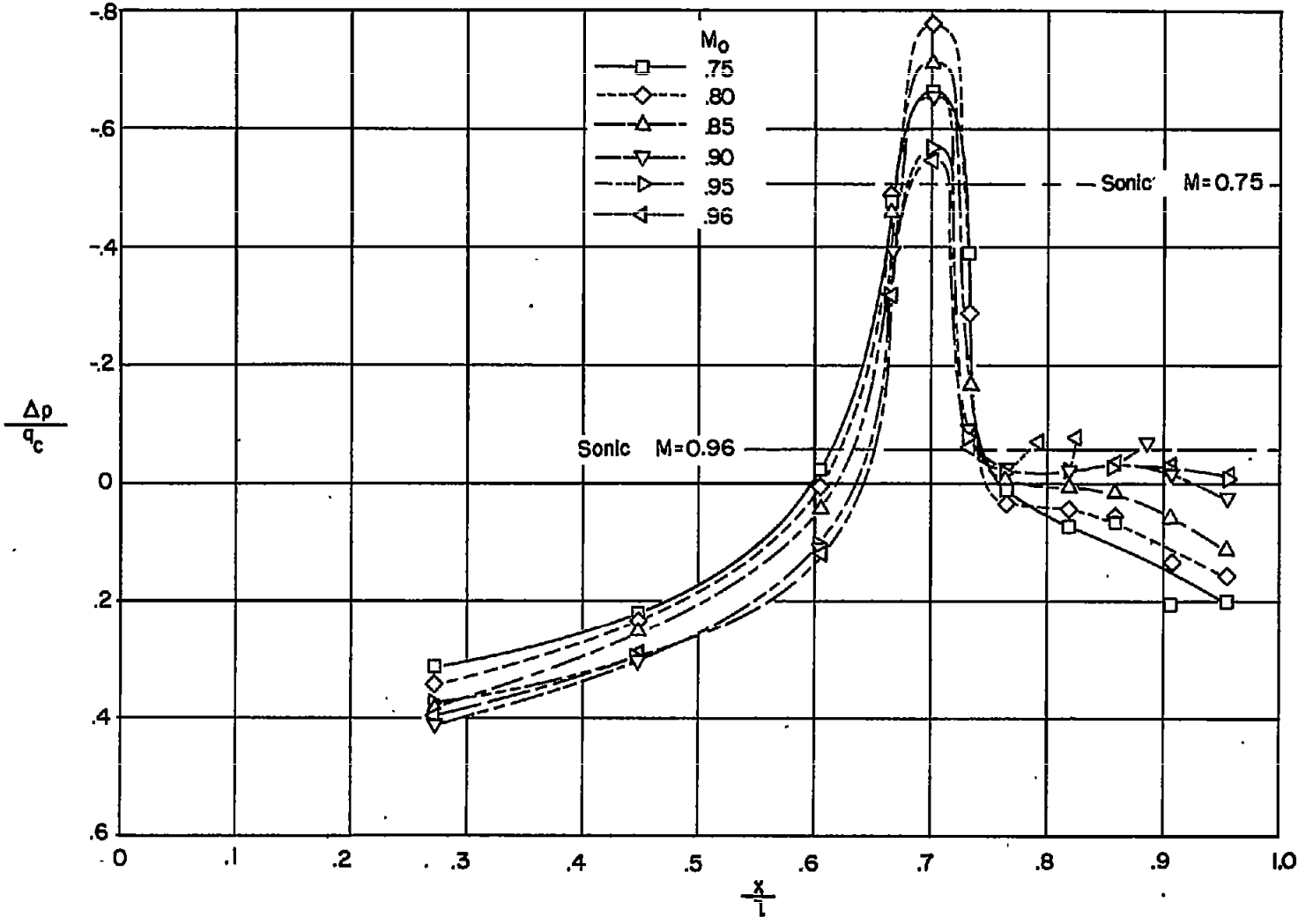

Figure 9.- Effect of Mach number on the pressure distribution over the surface of the 45° spherical spinner.

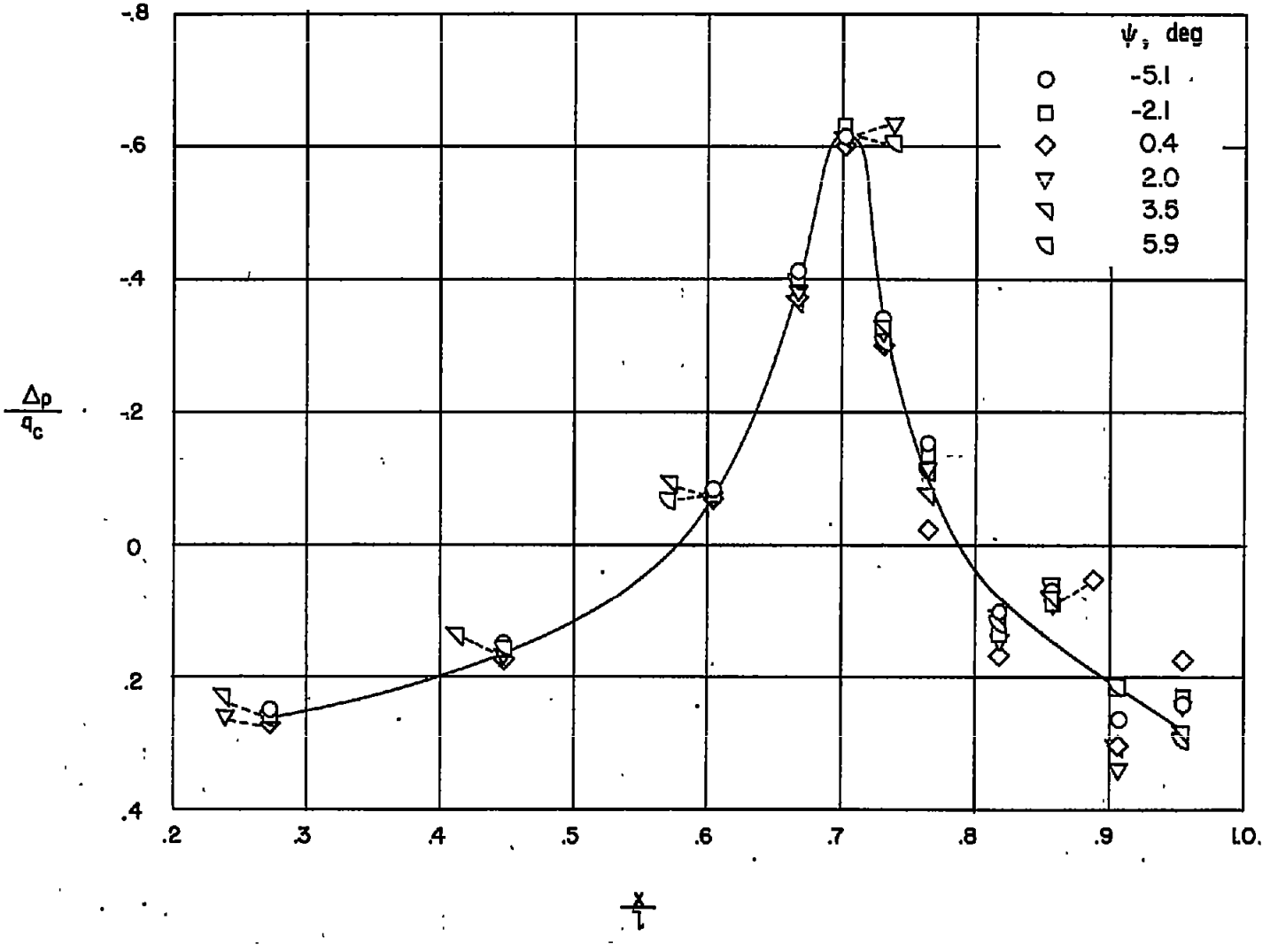

Figure 10.- Effect of yaw on the surface-pressure distribution of the 45° spherical spinner at M_o of 0.65.

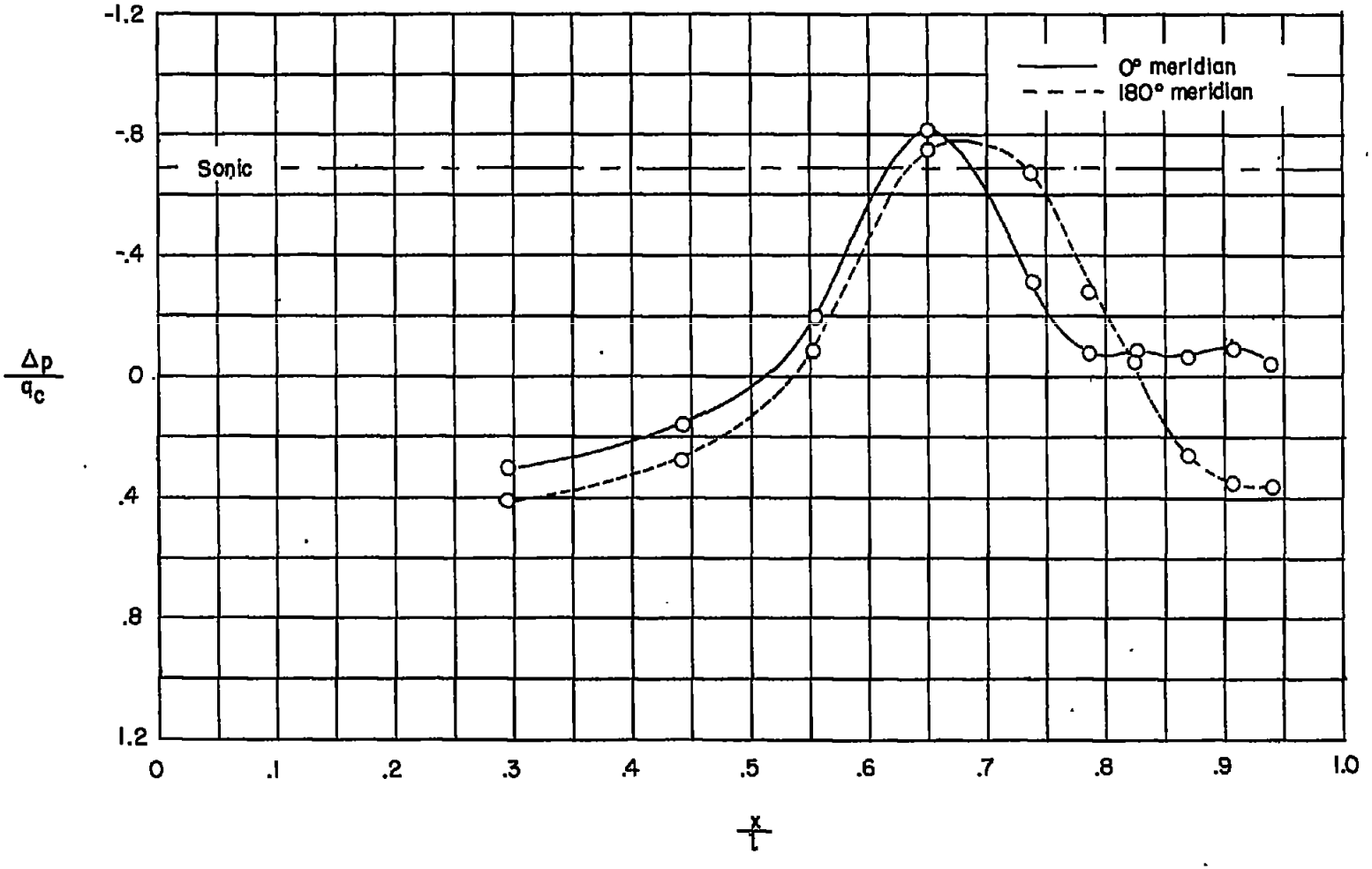

(a) $M_o = 0.70$.

Figure 11.- Effect of Mach number on the pressure distribution over the surface of the 60° spherical spinner.

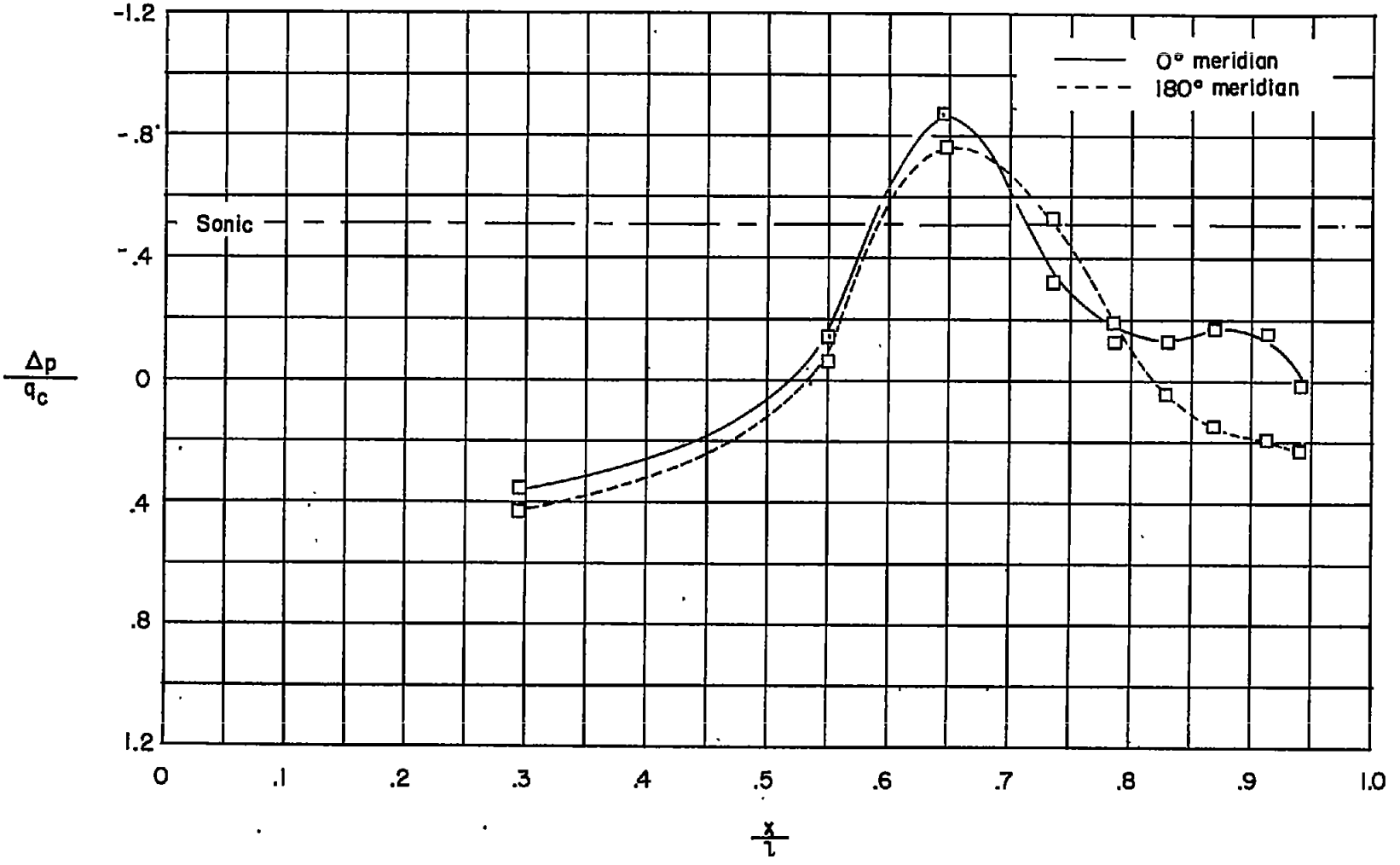

(b) $M_o = 0.75$.

Figure 11.- Continued.

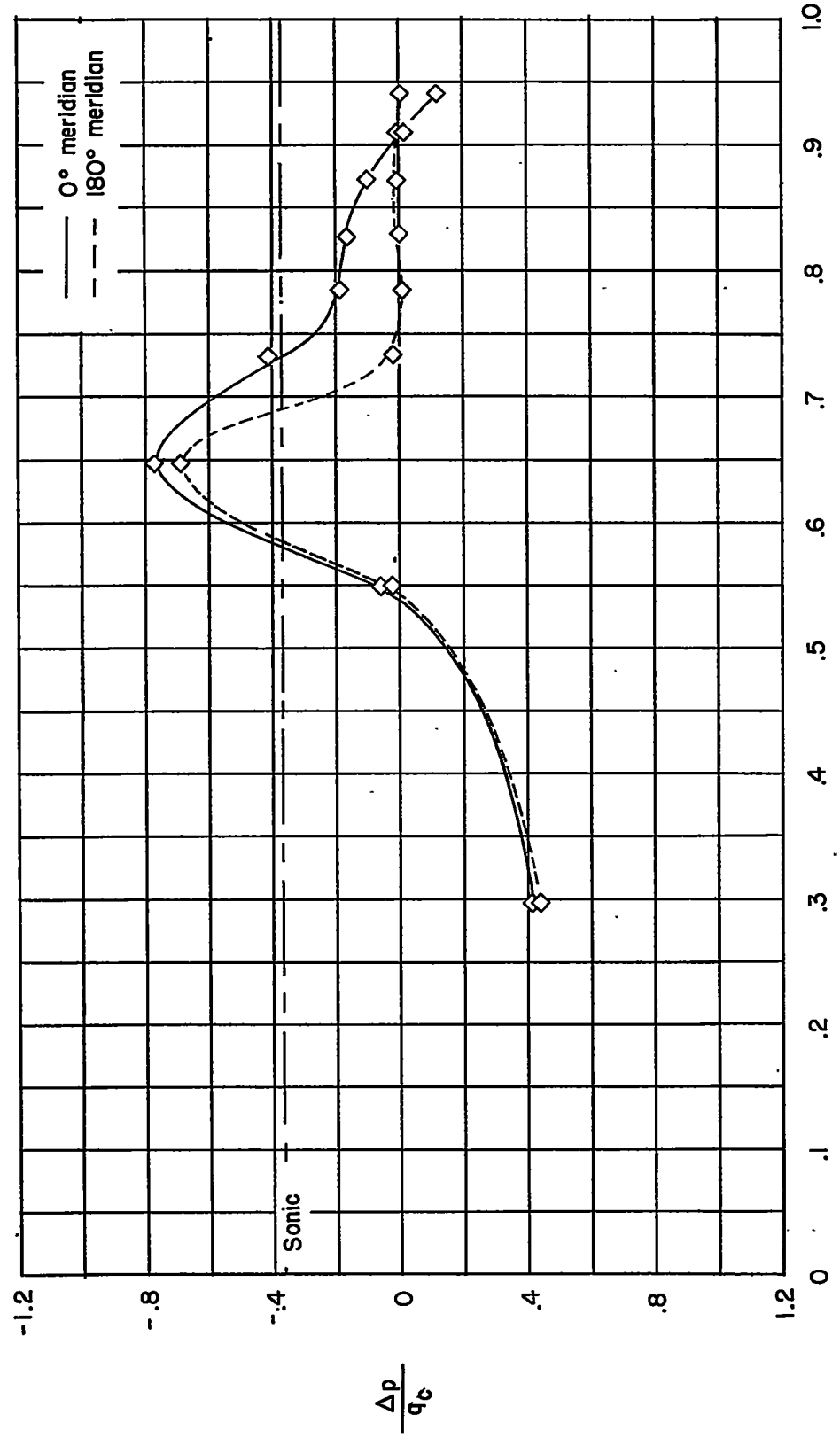

(c) $M_o = 0.80$.

Figure 11.- Continued.

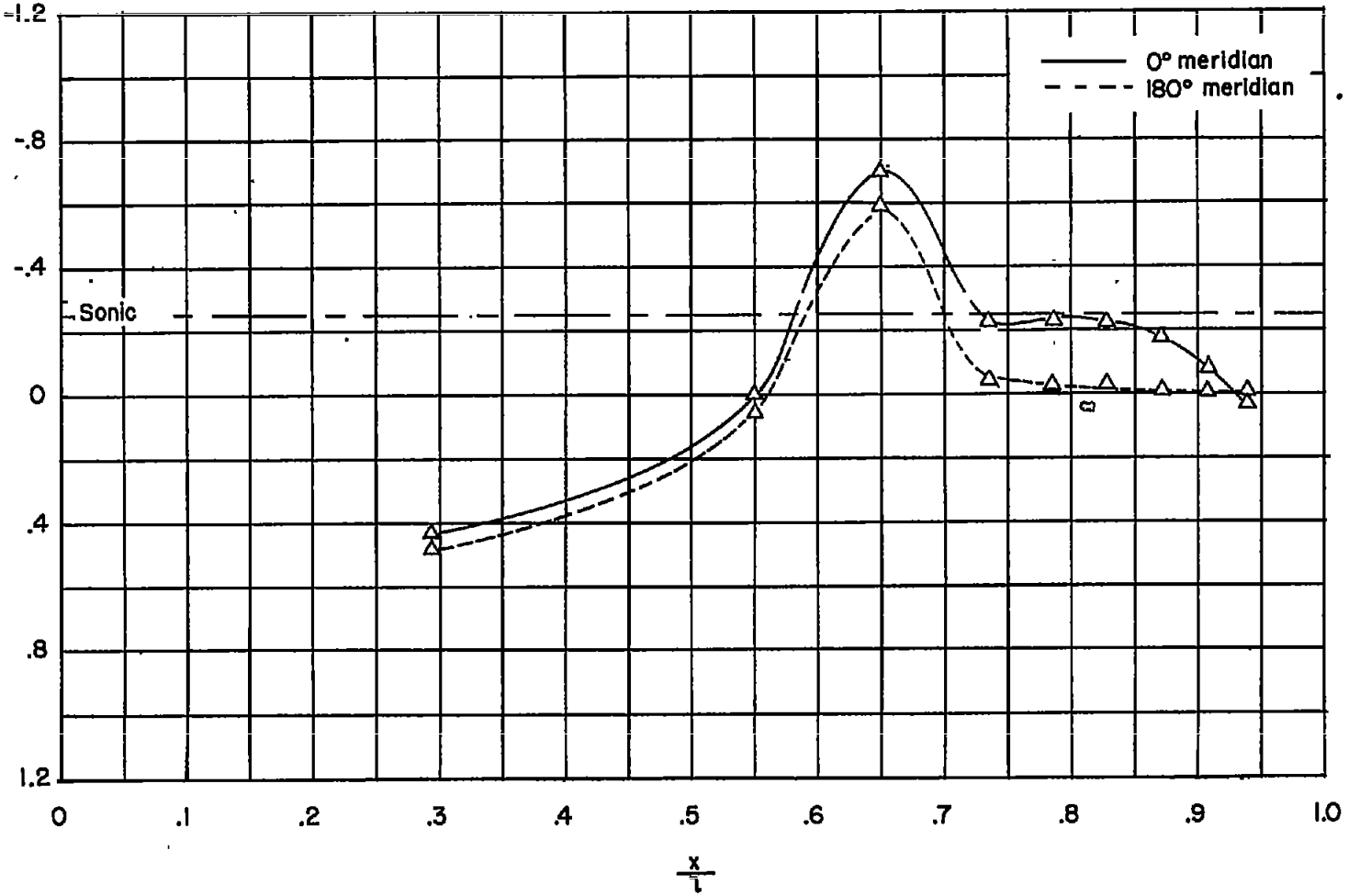

(d) $M_o = 0.85$.

Figure 11.- Continued.

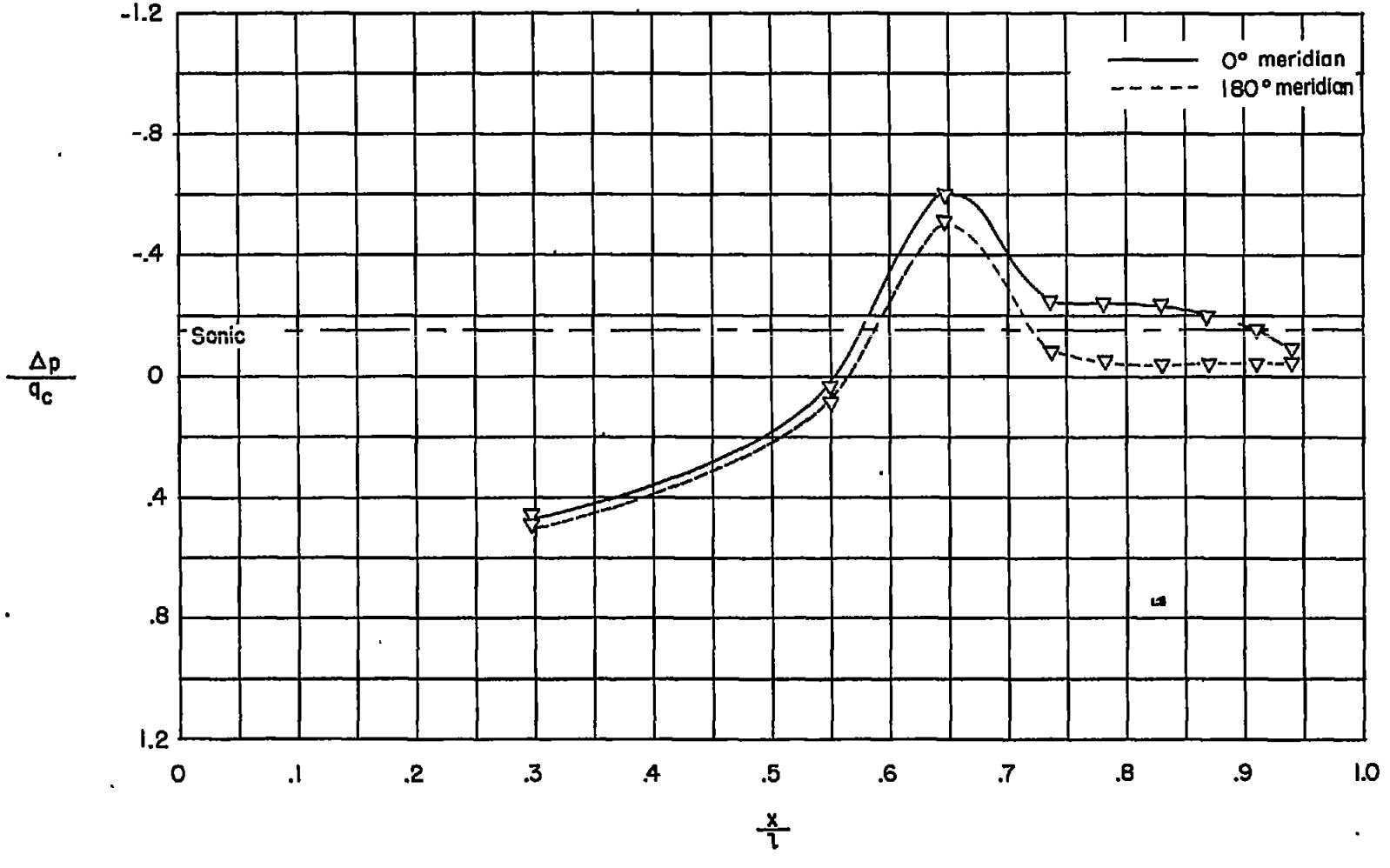

(e) $M_o = 0.90$.

Figure 11.- Continued.

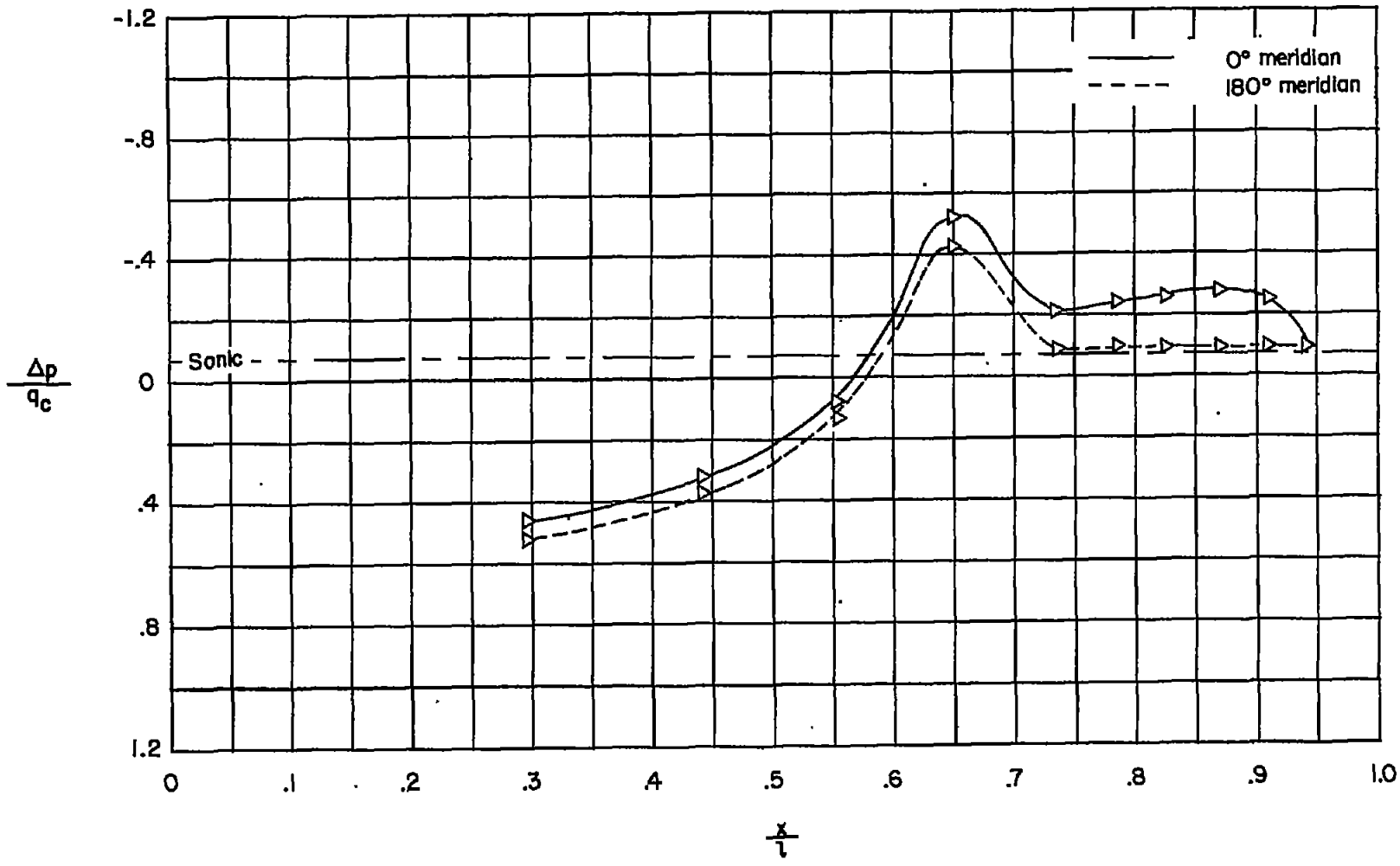

(f) $M_o = 0.95$.

Figure 11.- Concluded.

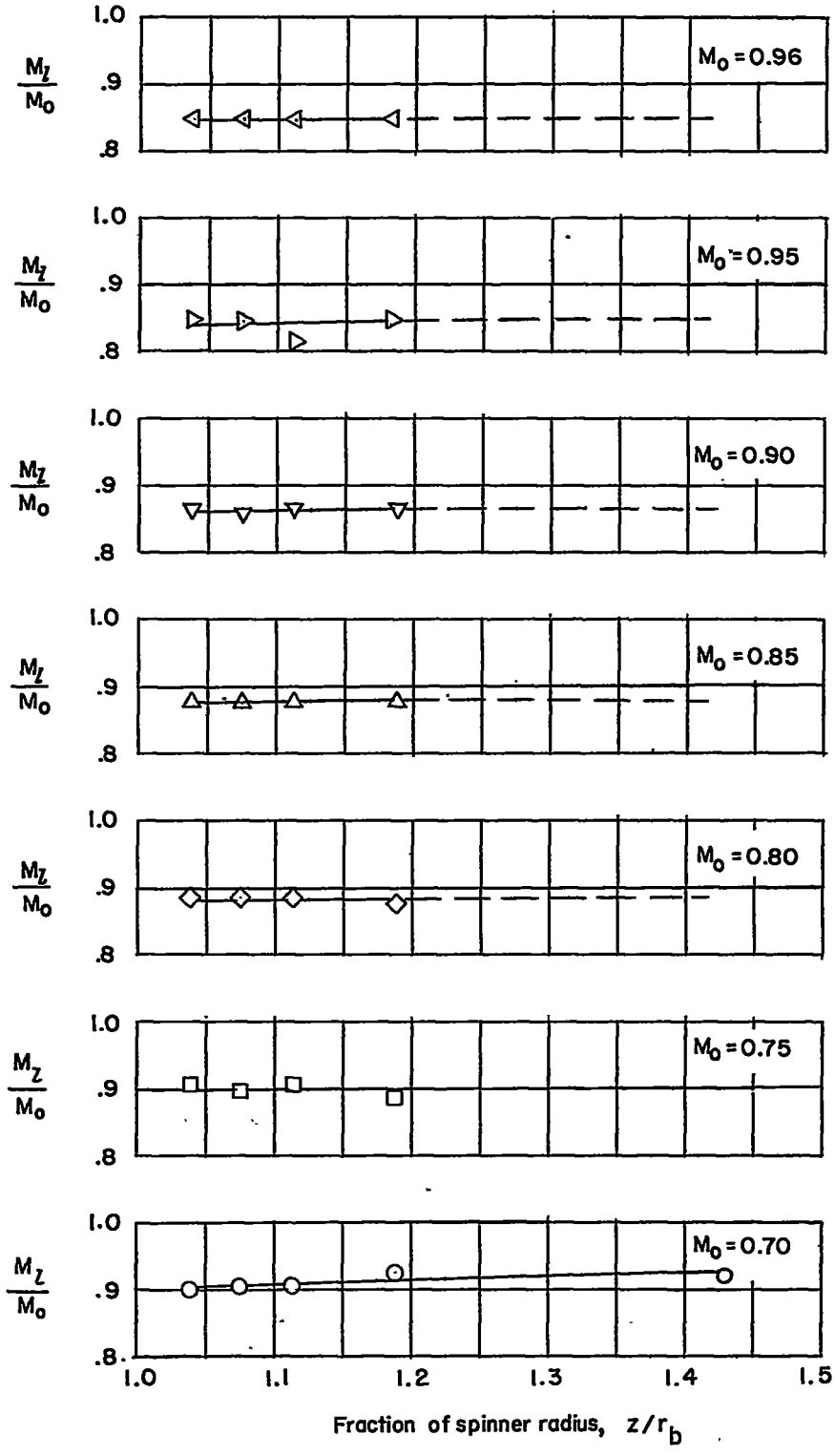

Figure 12.- Variation of local Mach number with radial distance. The conical spinner.

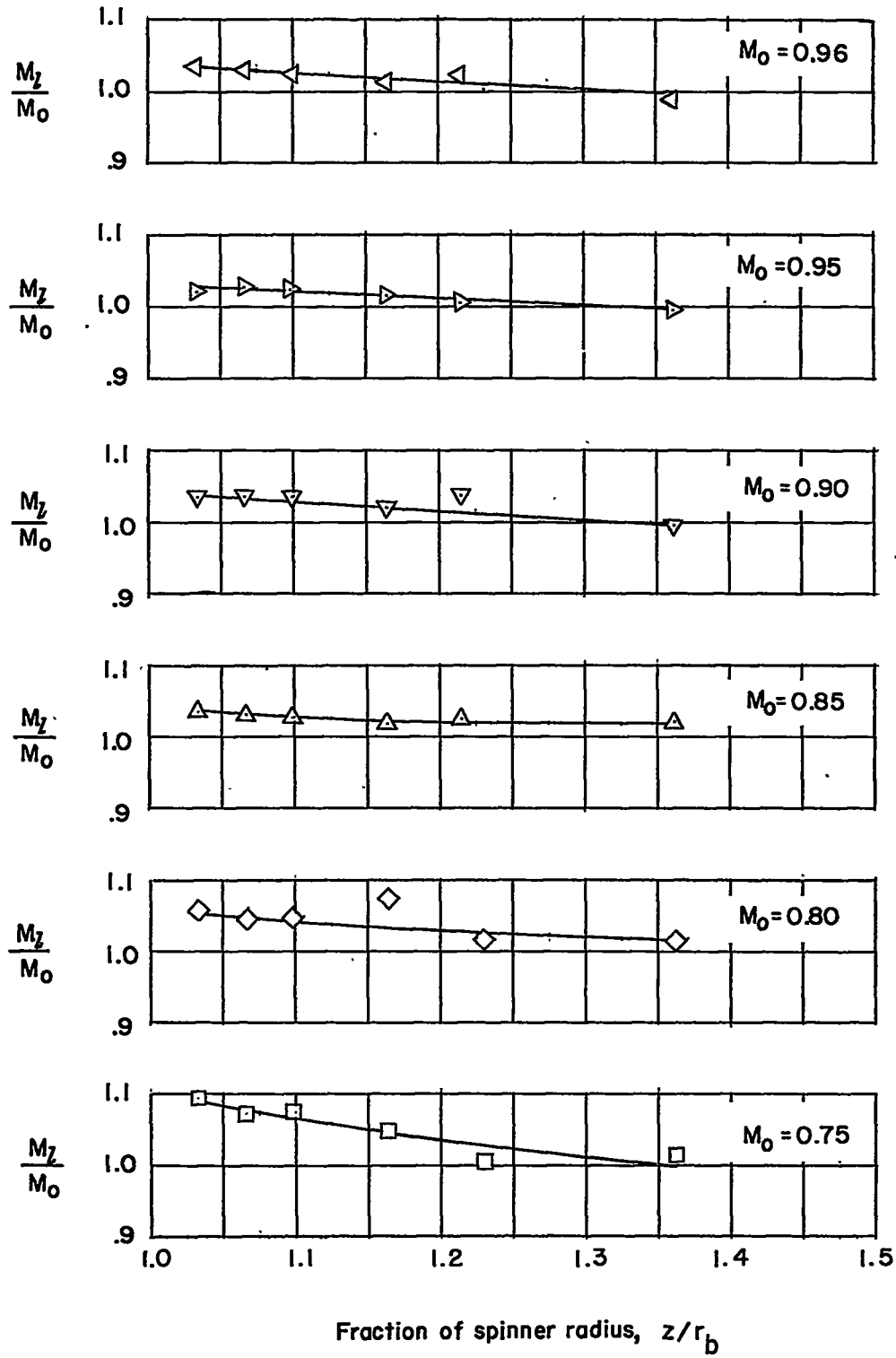

Figure 13.- Variation of local Mach number with radial distance. The 45° spherical spinner.

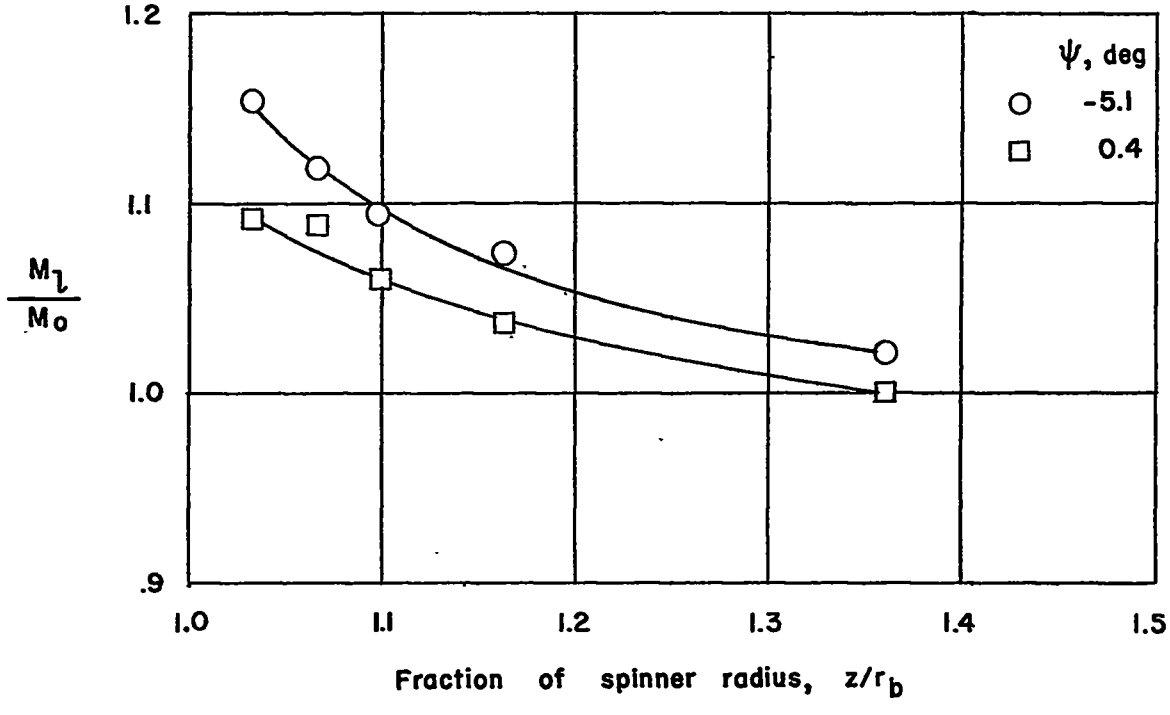

Figure 14.- Effect of yaw at M_o of 0.65 on the flow field at various values of spinner radius. The 45° spherical spinner.

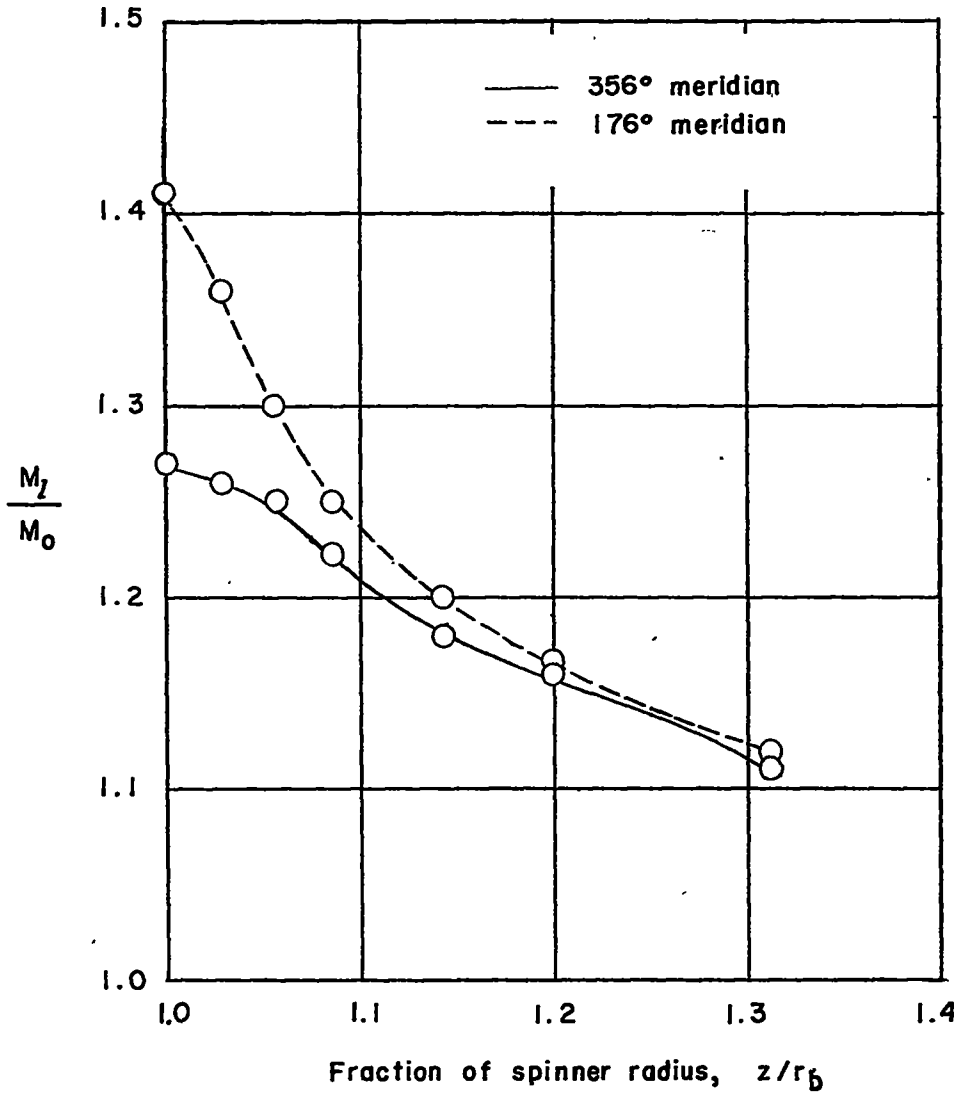

(a) $M_o = 0.70$.

Figure 15.- Variation of local Mach number with radial distance. The 60° spherical spinner.

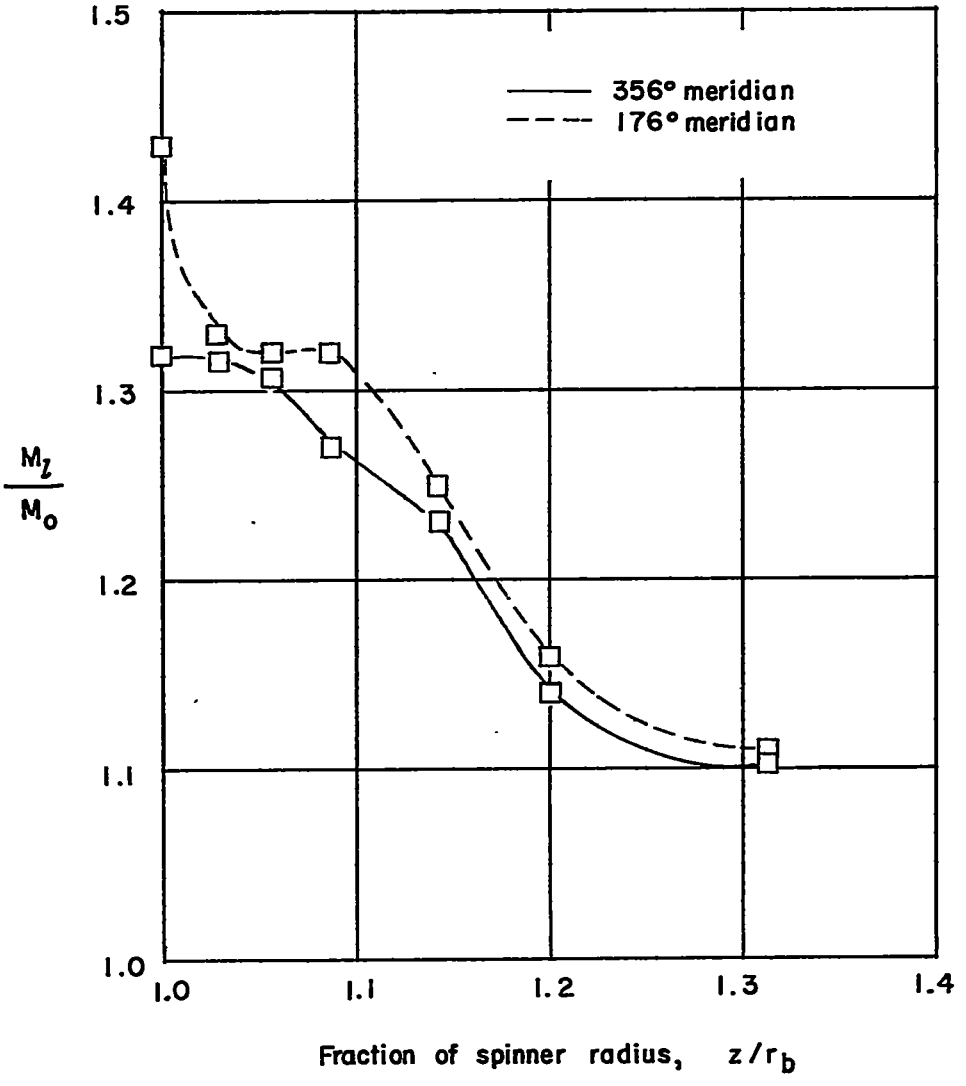

(b) $M_o = 0.75$.

Figure 15.- Continued.

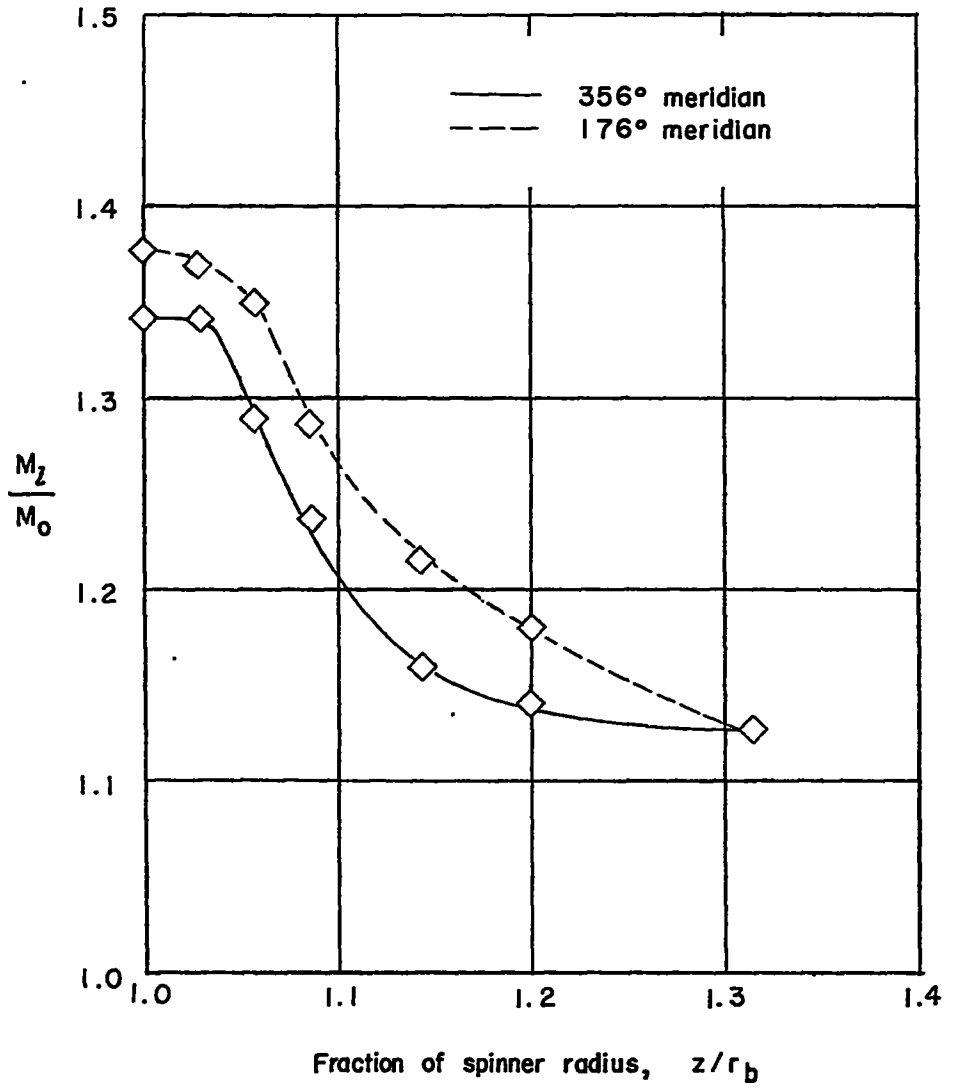

(c) $M_o = 0.80$.

Figure 15.- Continued.

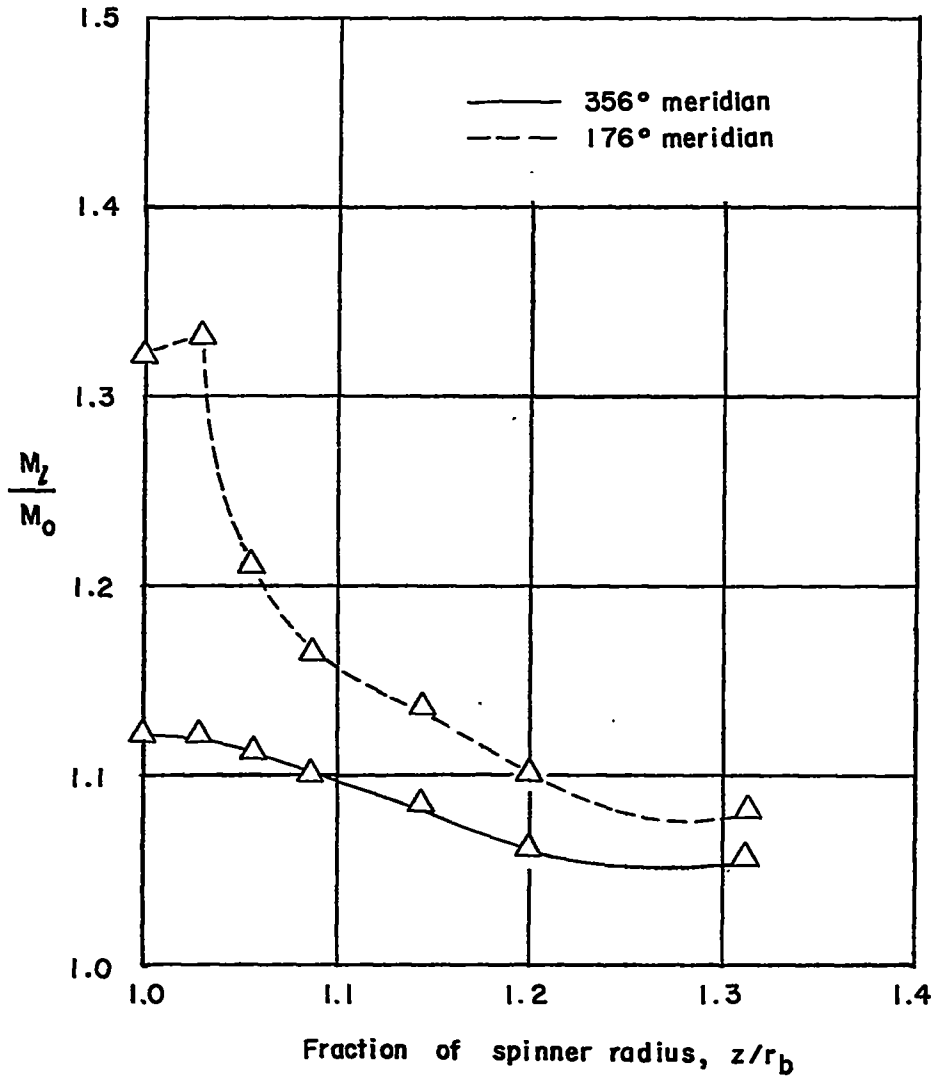

(d) $M_o = 0.85$.

Figure 15.- Continued.

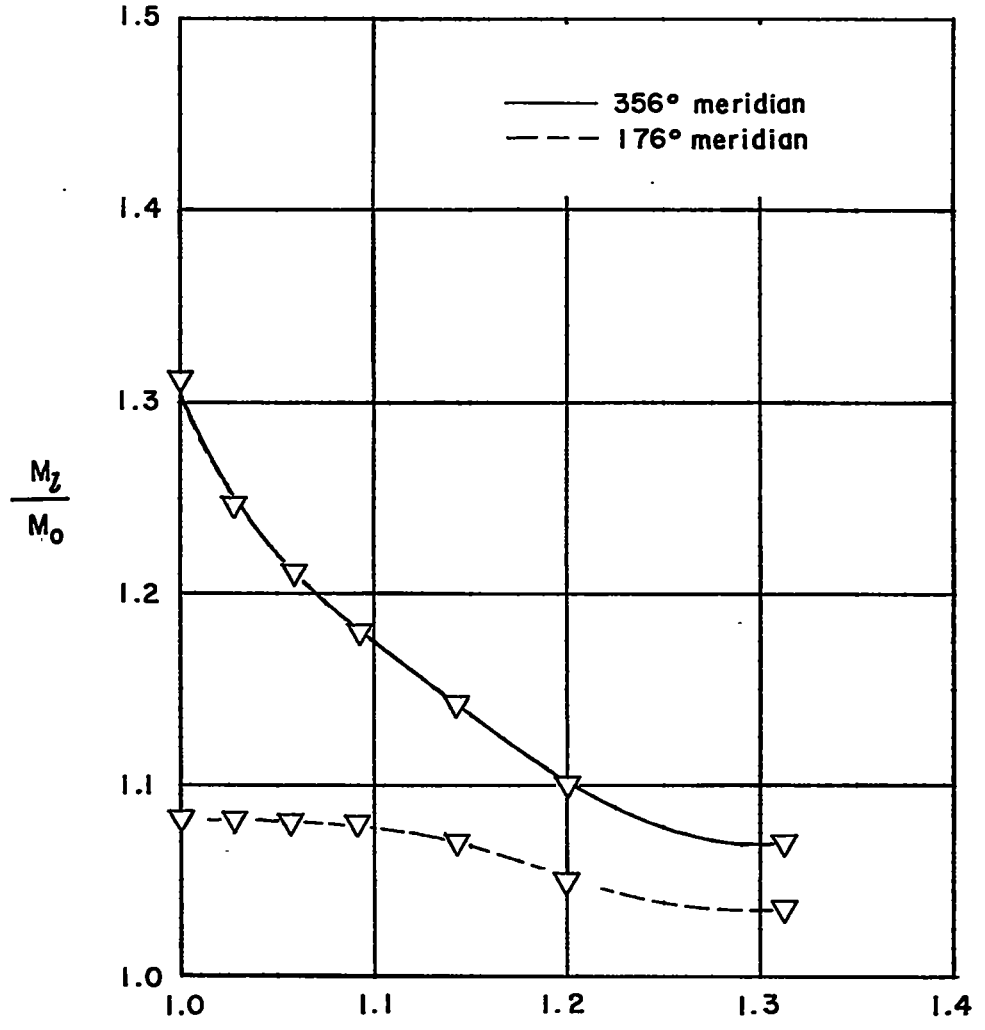

(e) $M_o = 0.90$.

Figure 15.- Continued.

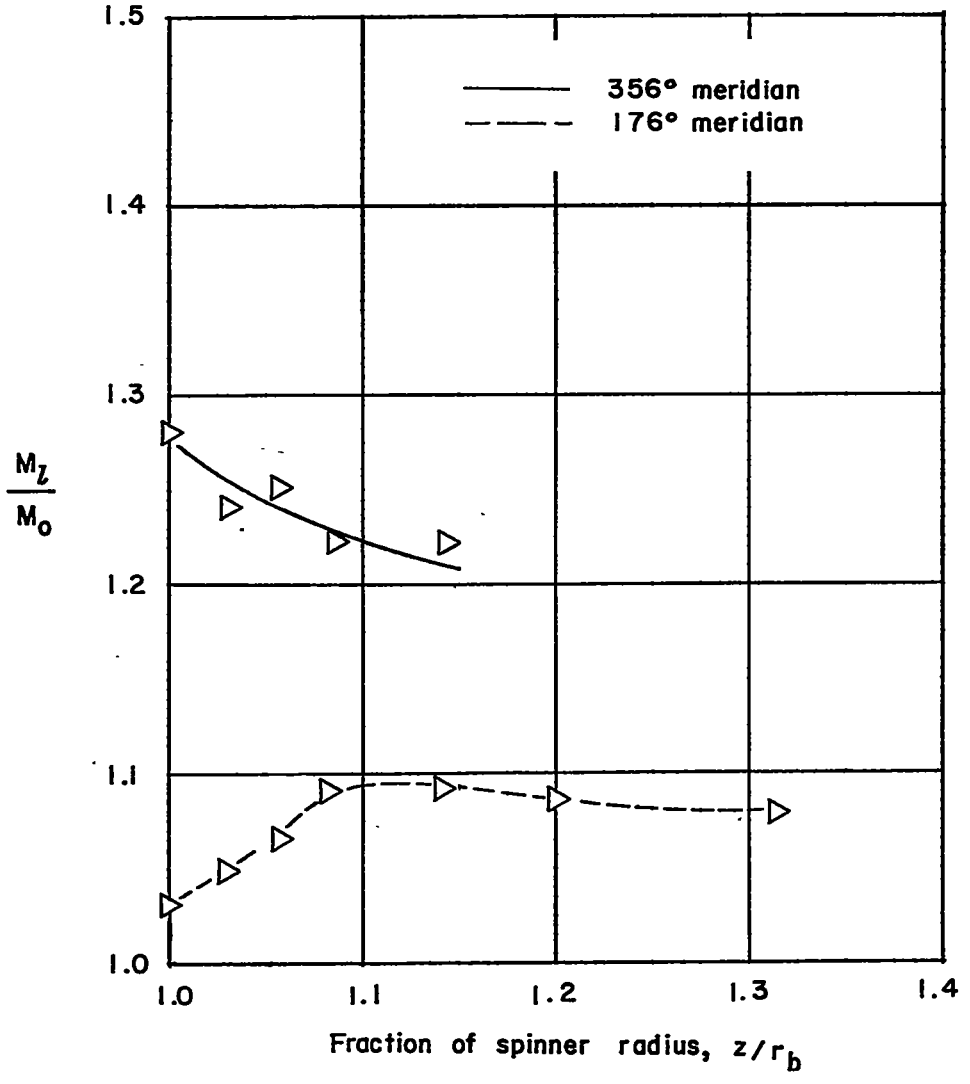

(f) $M_o = 0.95$.

Figure 15.- Concluded.